Gravity Wave and Turbulence Transport of Heat and Na in the Mesopause Region over the Andes

Yafang Guo[1], Alan Z. Liu[1,2], Chester S. Gardner[2]

[1]Center for Space and Atmospheric Research, Department of Physical Sciences, Embry-Riddle Aeronautical University, Daytona Beach, FL, USA.
[2]Department of Electrical and Computer Engineering, University of Illinois at Urbana-Champaign, IL, USA.

CEDAR Workshop
Poster MLTL-11

Abstract: The vertical heat and Na fluxes induced by gravity waves and turbulence are derived based on over 600 hours of observations from the Na wind/temperature lidar located at the Andes Lidar Observatory (ALO), Cerro Pachòn, Chile (30.2°S, 70.7°W). In the 85-100 km region, the annual mean vertical fluxes by gravity waves show downward heat transport with a maximum of 0.78 K m/s at 90 km, and downward Na transport with a maximum of 120 m/s/cm^3 at 94 km. The vertical heat flux due to turbulence eddies are also derived with a novel method that relates turbulence fluctuations of temperature and vertical wind with photon count fluctuations at very high resolutions (25m, 6s). The results show that the vertical transport is comparable to those by gravity waves. The eddy diffusivity is also estimated from the direct measurement of eddy fluxes.

Introduction

It is well recognized that gravity waves (GWs) play important roles in establishing the general circulations and thermal structure of the upper mesosphere and lower thermosphere (MLT). Gravity waves experience increasing amplitudes and tendency for instabilities as they propagate upward through the decreasing atmospheric density. Nonlinear wave interactions and dynamical and convective instabilities are some typical mechanisms that cause wave saturation and breaking. Gravity waves contribute to the vertical transport of heat and atmospheric constituents by inducing advection, turbulent mixing, dynamical transport, and chemical transport. These four mechanisms can substantially affect the chemistry and thermal structure of atmosphere in the mesosphere. Gravity waves also have an associated energy flux, and for non-conservative waves, their energy dissipation generates local heating in the MLT. Here we are focusing on the effects of dissipating and breaking gravity waves on the thermal and constituent structure of the mean circulation.

Observational Data

1. Data Summary

The data used in this research is the Na lidar measurements of vertical wind, temperature and Na density made in the mesopause region between 80 km and 105 km. The lidar is located at Andes Lidar Observatory (ALO) in Cerro Pachòn, Chile (30.2°S, 70.7°W). Since the lidar was deployed at ALO in 2009, it was operated on a campaign based 3-4 times per year with about 2 weeks for each campaign. In May 2014 a major upgrade of the lidar system resulted in a significant improvement of the signals as well as the system's stability. Several campaigns were conducted after the upgrade, which acquired more data than all previous campaigns and with much better quality. In this study, both data before and after the upgrade are used.
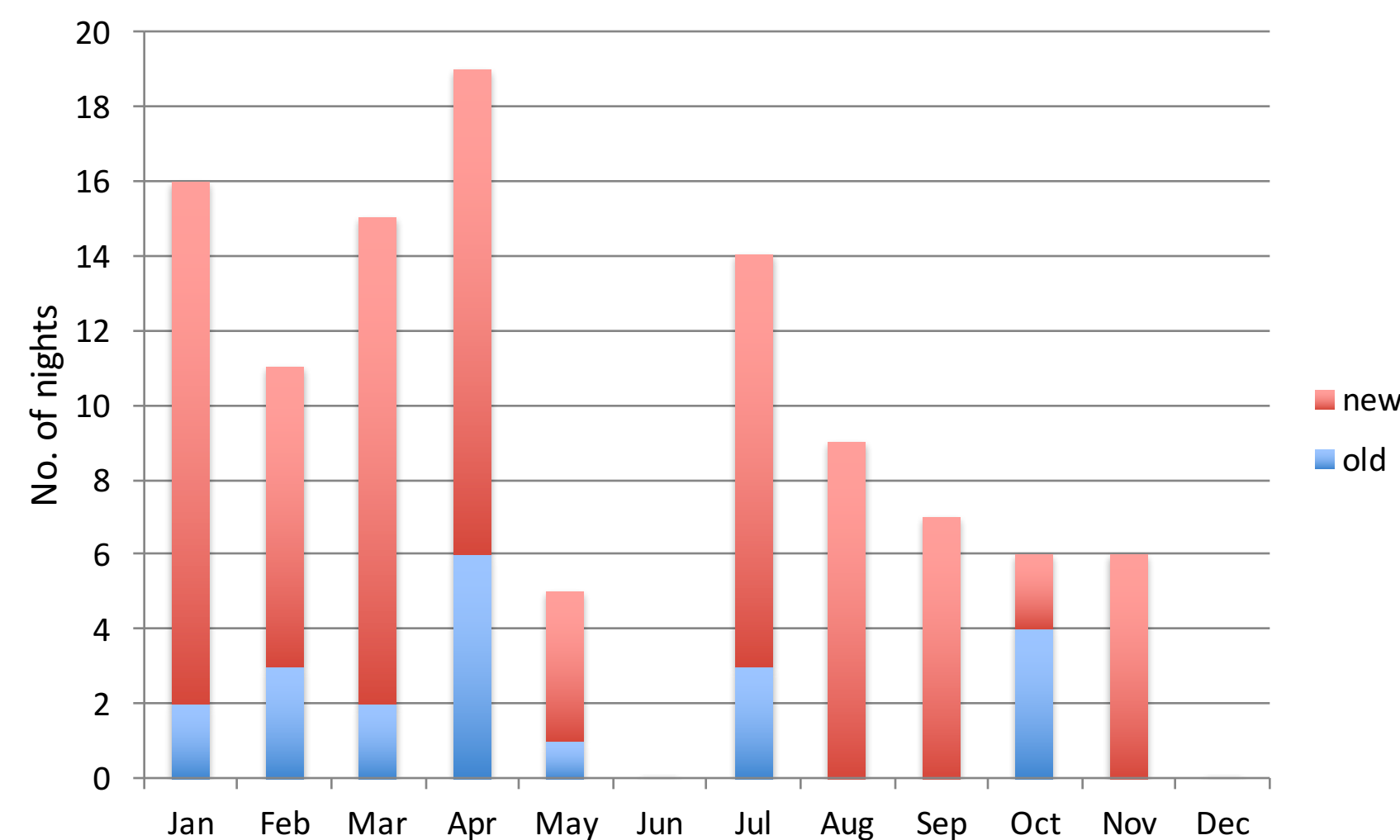

Fig 1. Na lidar data summary including old and new data, total number of nights is 108, with 21 nights of old data, 87 from new data.

Table 1. Summary of lidar operation modes and data resolutions after upgrade describes how lidar data is acquired and processed for all the campaigns since upgrade. The 'description' column denotes the operating mode and raw data integration time. For example, 'ZSZ' indicates that the sequence of directions that laser beam was pointed to is Zenith-South-Zenith-East, and '6s x10' means that the data was collected with 6s integration time for each profile and 10 profiles consecutively in each direction before moving to the next direction. In post processing, the raw data profiles are combined to 30, 60, or 90 seconds integration time with 500 m vertical resolution before used to derive temperature and winds. This temporal and vertical resolutions are chosen so the derived temperature and wind have acceptable uncertainties due to photon noise.

Date	Description	Processed Data
May 2014	Z, 6s; Z, 30s	90s, 500m
Aug-Sep 2014	Z, 3s; Z, 6s	90s, 500m
Jan-Feb 2015	Z, 3s; Z, 6s; ZSZE, 90s	90s, 500m
Apr 2015	Z, 6s; ZSE, 6s x 10	60s, 500m
Jul 2015	ZSE, 6s x 10	60s, 500m
Oct-Nov 2015	Z, 6s; ZSZE, 6s x 10	60s, 500m
Feb-Mar 2016	ZSZE, 3s x 10; ZSZE, 6s x 10	30s/60s, 500m

Gravity Wave Vertical Fluxes

According to polarization relationship in the linear gravity wave theory, temperature and wind perturbations (T' and w') are near orthogonal without dissipation. The heat flux is characterized as covariance between temperature and wind perturbations (T' and w'). The vertical heat flux becomes non-zero when gravity waves dissipate, and T' and w' become non-orthogonal. The vertical transport caused by dissipating gravity waves is typically downward in the mesopause region, which brings cooling effect to the region where wave dissipation occurs.

Because of different signal levels, the temperature and winds using old data were derived typically at 1 km and 270 s for vertical and temporal resolutions, respectively. The integration time and altitude intervals for the new data is summarized in Table 1. Due to large geophysical fluctuations of T and w, long term average is required to reduce the uncertainty of the vertical fluxes.
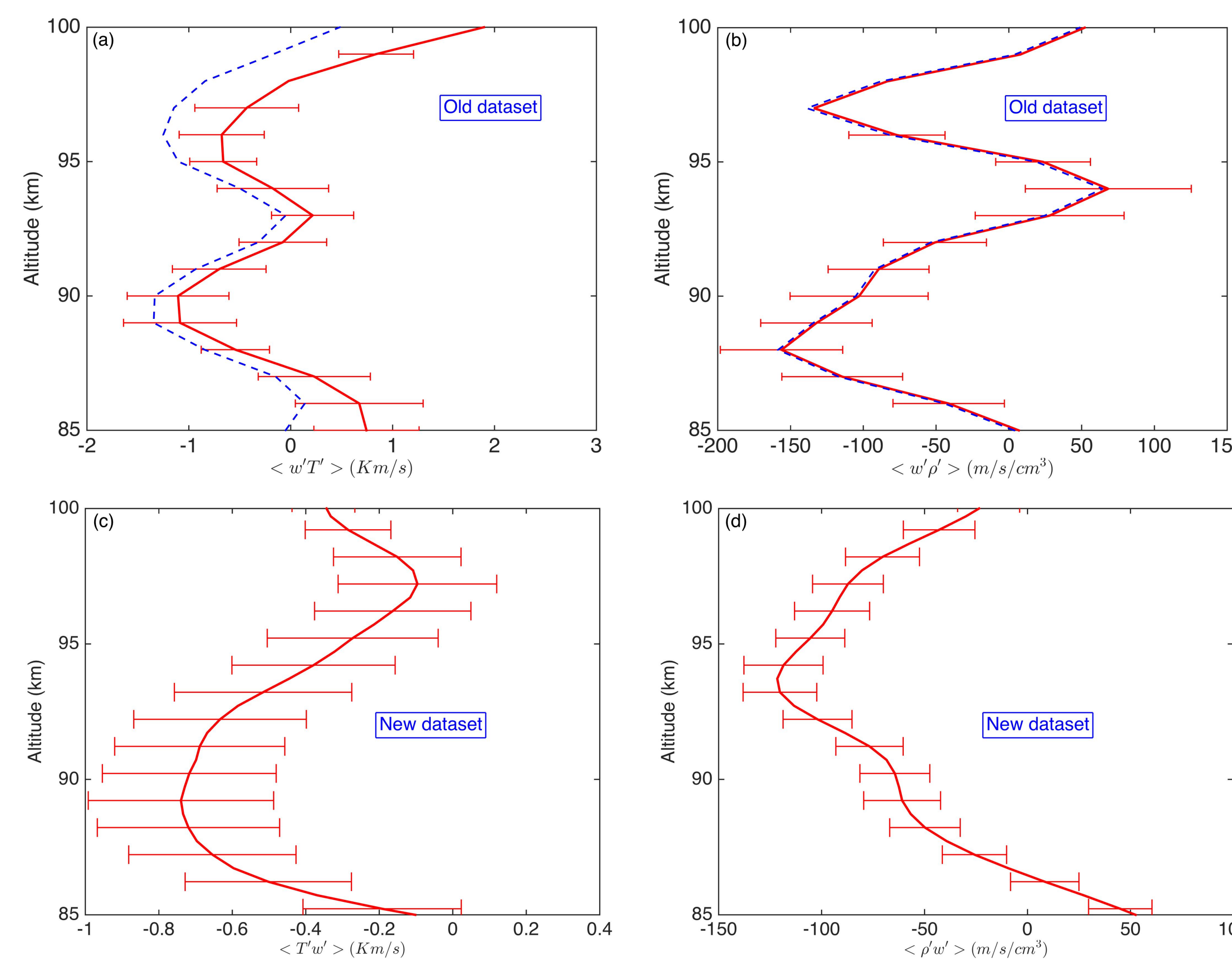

Fig 2. Heat (<w'T'>) and Na (<w'ρ'>) fluxes from both old and new data. (a) and (b) are results of vertical fluxes averaged over 21 nights and 100 hours of zenith measurements. (c) and (d) are from new data with over 80 nights and 320 hours zenith measurements. The solid red and dashed blue lines in (a) and (b) are vertical fluxes with and without bias removed. The heat flux bias, calculated according to *Gardner and Vargas* [2014], ranges from -0.2 K m/s at the center of Na layer (≈92 km) to -0.8 K m/s near the top and bottom.

Eddy Heat Flux and Eddy Thermal Diffusivity
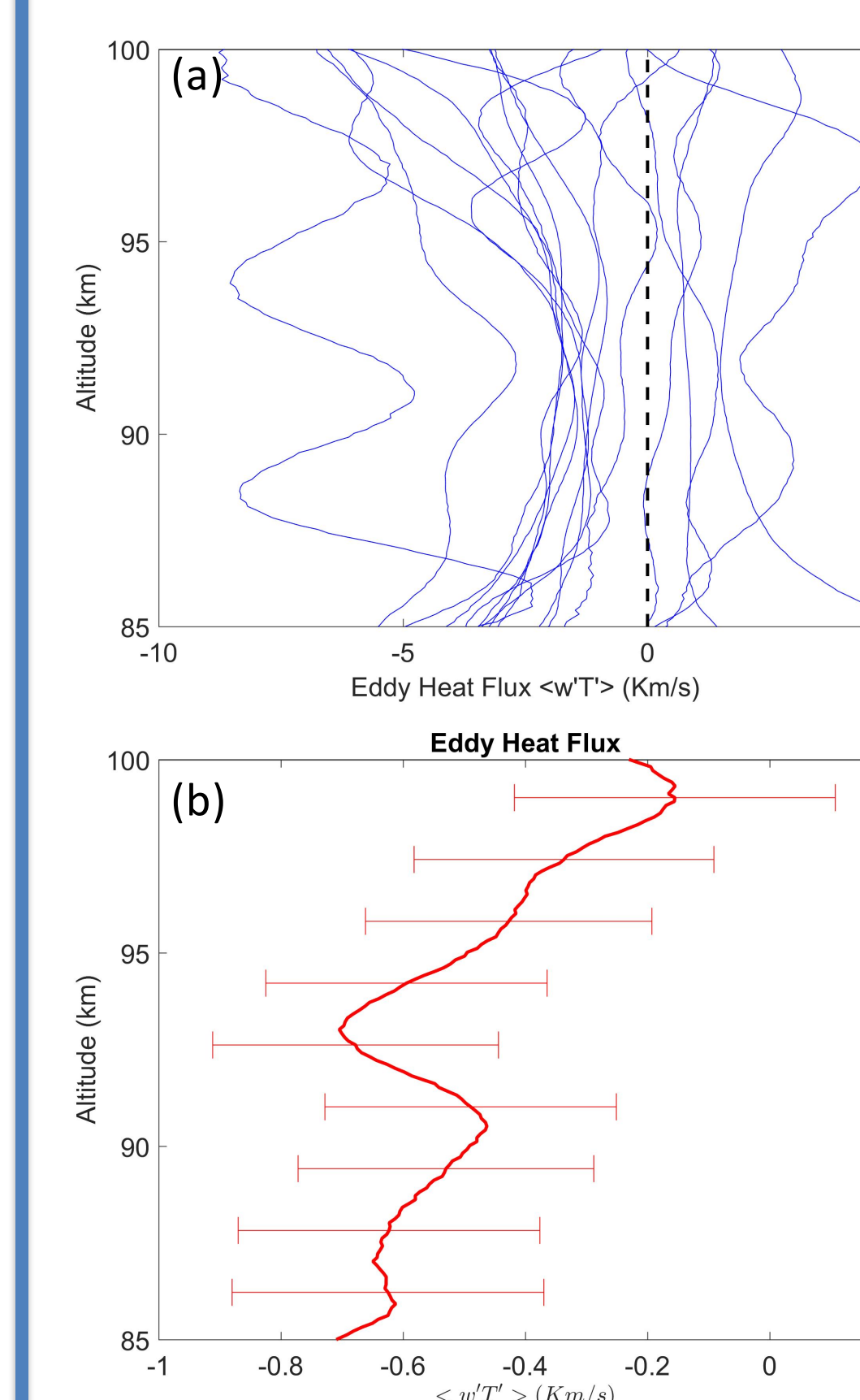
Similar to calculating GW flux, there is also a bias related to photon count noise in turbulence flux calculations. This bias can be eliminated by applying different sets of photon counts to temperature and wind perturbation. Here the method we use to remove bias is: the wind perturbations (w') in time t_1 is multiplied by temperature perturbation (T') in next time interval t_2, and w' in t_2 is multiplied by T' in t_1, and the rest of the heat flux profiles are calculated with the same scheme. The instantaneous heat fluxes are averaged through the night. The fluxes from all nights are then averaged to obtain the mean eddy heat flux profile.

The eddy thermal diffusion coefficient (k_H) can be calculated from measured eddy heat flux, which is defined as:

$$k_H = \frac{-\overline{w'T'}}{\Gamma_{ad} + \partial \bar{T}/\partial z}$$

Fig 3. (a). Nightly mean heat flux profiles on 24 nights from May 2014 to July 2015. (b). The mean eddy heat flux averaged over all the nights in (a). (c) Mean eddy thermal diffusion coefficient (k_H). The maximum is about 85 m^2/s at around 93 km
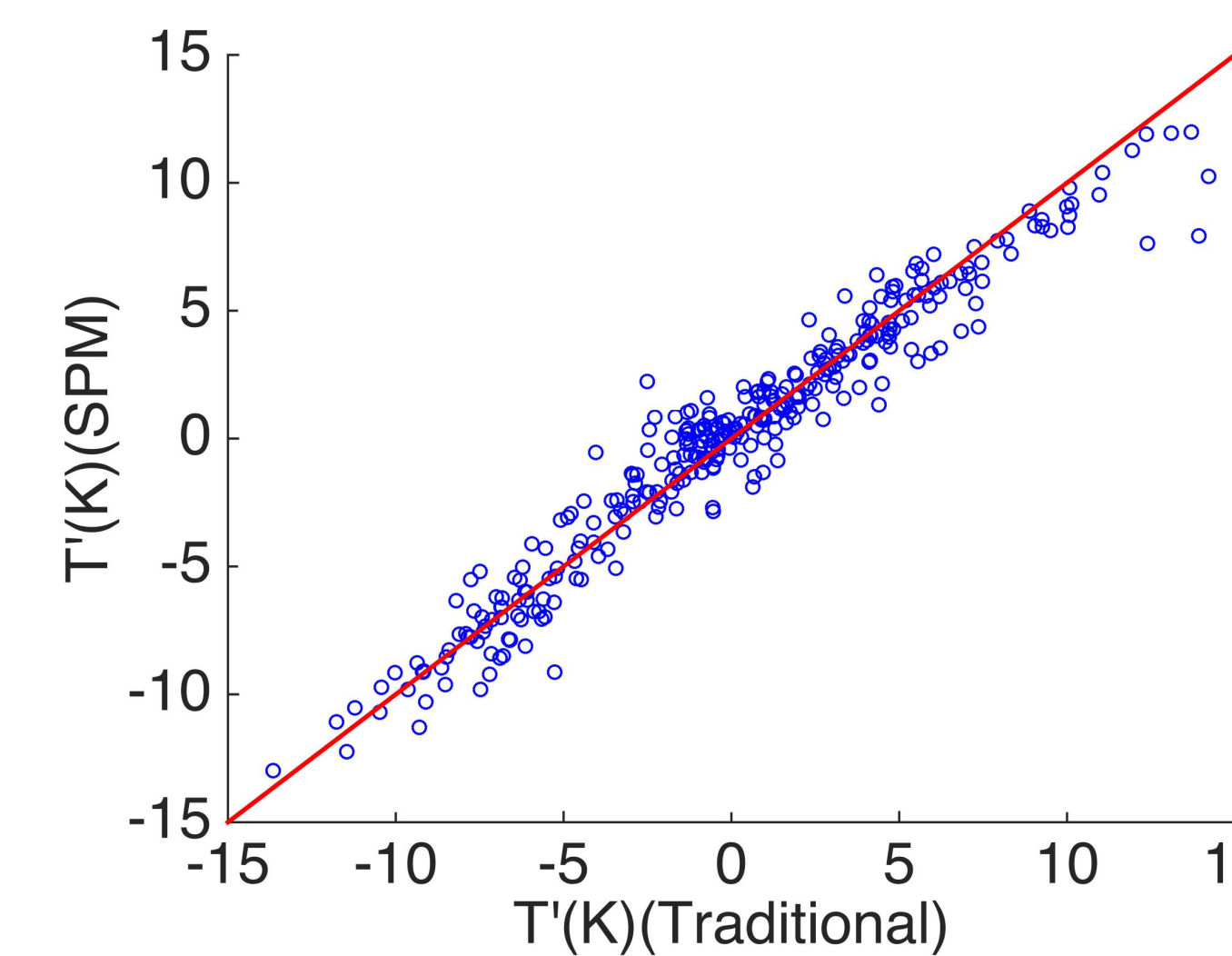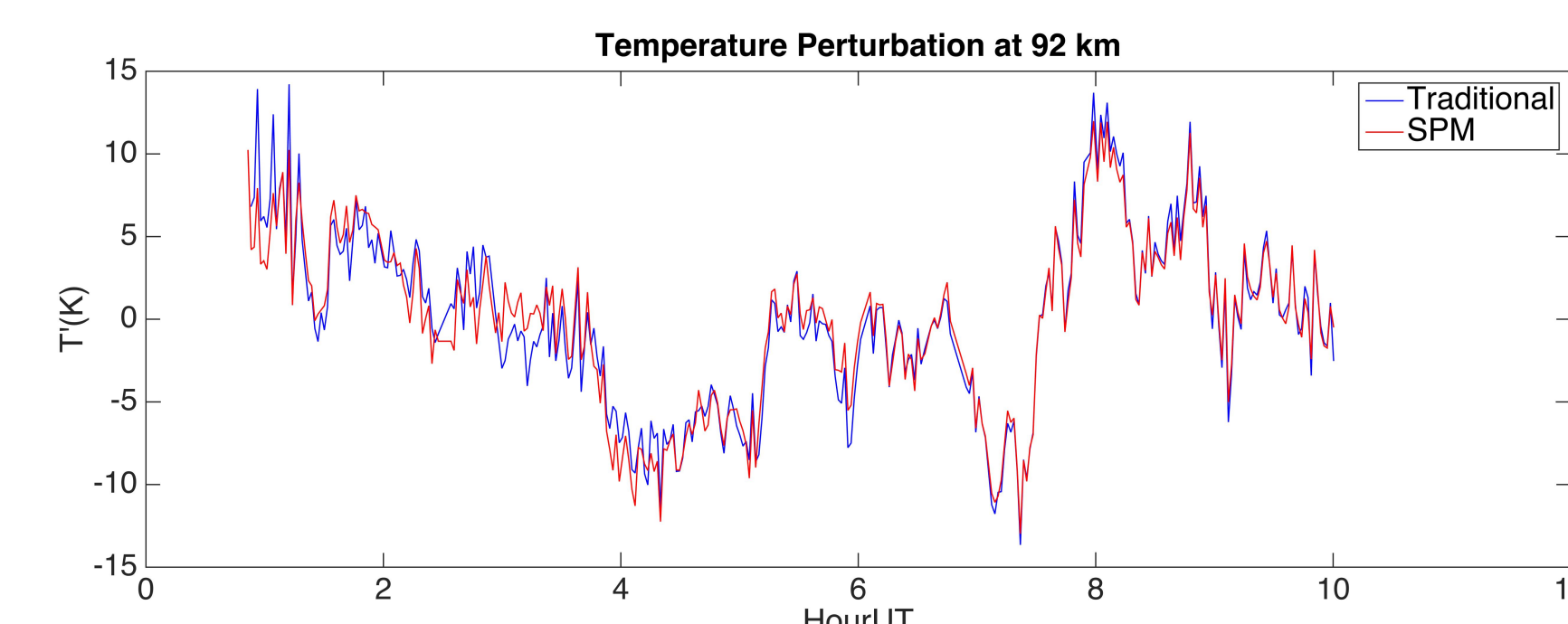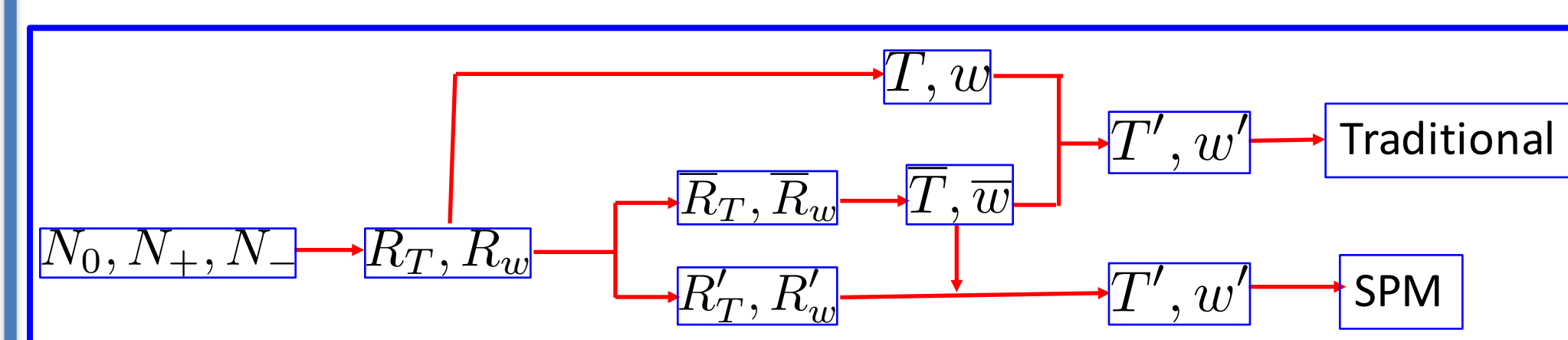
Conclusion

➢ The vertical heat fluxes induced by gravity waves are derived using over 600 hours Na lidar data. These transports play significant role in the atmospheric thermal structure and constituent distribution.

➢ A new method to derive turbulent perturbations is proposed and applied to for eddy flux calculation and turbulence studies.

➢ Eddy heat flux and eddy thermal diffusivity are calculated for the first time from direct measurements with lidar data.

Signal Perturbation Method (SPM)

Gravity wave perturbations can be derived directly from temperature, wind, and Na density at 60 s and 500 m resolutions as traditional method. In this study, a method is developed by using the signal ratios (R_T and R_w) for turbulent perturbations instead of the raw photon counts. The density perturbation is calculated directly from photon count fluctuations. This is because R_T and R_w are directly related to T and w while the Na density fluctuation is related to the absolute photon count fluctuations. R_T and R_w are defined as Eq. (1), then the perturbations can be derived through Eq. (2).

$$R_T = \frac{N_+ + N_-}{N_0} \qquad R_T' = \left.\frac{\partial R_T}{\partial T}\right|_w T' + \left.\frac{\partial R_T}{\partial w}\right|_T w' \quad (2)$$

$$R_w = \frac{\ln(N_-/N_+)}{\ln(N_-N_+/N_0^2)} \qquad R_w' = \left.\frac{\partial R_w}{\partial T}\right|_w T' + \left.\frac{\partial R_w}{\partial w}\right|_T w'$$

(1)

In order to verify the perturbations derived from SPM, results are compared with traditional method followed by the flow chart here. The scatter plot (top) and time series plot (left) are the temperature perturbations comparisons. They match well in terms of the gravity wave scale.
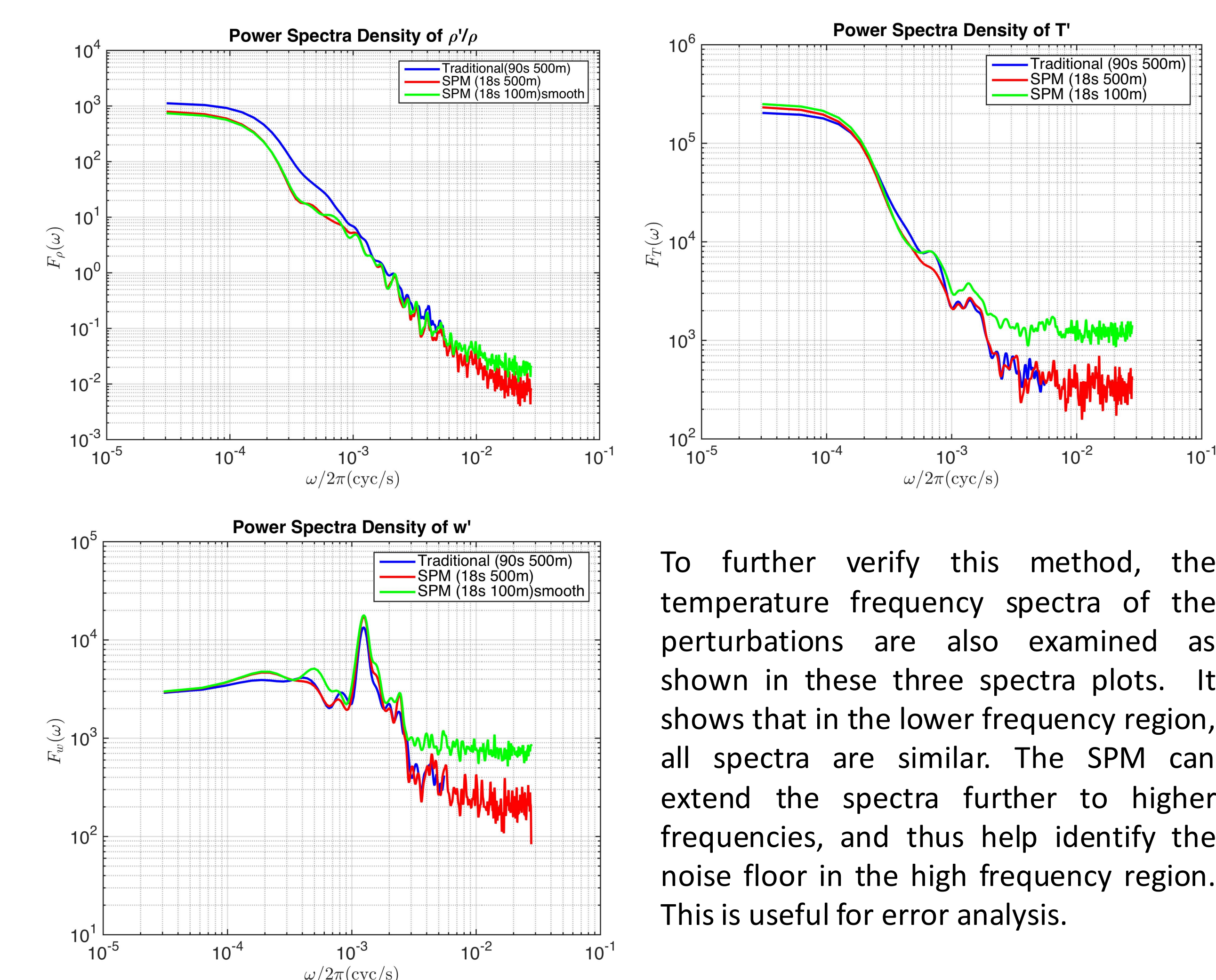
To further verify this method, the temperature frequency spectra of the perturbations are also examined as shown in these three spectra plots. It shows that in the lower frequency region, all spectra are similar. The SPM can extend the spectra further to higher frequencies, and thus help identify the noise floor in the high frequency region. This is useful for error analysis.

guoy1@my.erau.edu Yafang Guo